AIAA JOURNAL
Vol. 45, No. 9, September 2007

Structure of Plumes from Burning Aluminized Propellant Estimated Using Fan Beam Emission Tomography

Yudaya Sivathanu* and Jongmook Lim†
En'Urga Inc., West Lafayette, Indiana 47906
and
Laurence E. Reinhart‡ and Robert C. Bowman Jr.§
Jet Propulsion Laboratory, California Institute of Technology, Pasadena, California 91109

DOI: 10.2514/1.28742

Fan beam emission tomography in the 1–5-μm band is used to estimate the structure of a solid rocket propellant plume. Fan beam emission tomography consists of two components. The first is a pair of orthogonal high-speed imaging spectrometers and scanners that measures the spectral radiation intensities from 1.3 to 4.8 μm at 256 view angles. The second is a robust deconvolution algorithm that estimates the structure of the plume from the spectral radiation intensity measurements. The deconvolution algorithm is based on the maximum likelihood estimation method in conjunction with a linearized radiative transfer equation. The radiation intensity measurements were completed in a series of burns using 2.5-cm-diam by 1.25-cm-long strands of aluminized solid rocket composite propellant. In general, the aluminum diffusion-flame particulate temperatures in the plume are much higher than the gas temperatures. The gaseous combustion product concentrations are much lower in the middle of the plume than at the outer edges. This indicates a diffusion-flame-type structure for the plume, caused by the fact that the composite solid rocket propellant is fuel-rich. The results indicate that reliable plume-structure measurements can be obtained using fan beam emission tomography.

Nomenclature

d	=	diameter of the burning surface, cm
I_λ	=	spectral radiation intensity, $W/(m^2 \cdot sr \cdot mm)$
$I_{\lambda b}$	=	blackbody spectral radiation intensity, $W/(m^2 \cdot sr \cdot mm)$
T	=	temperature, K
X_{CO_2}	=	carbon dioxide mole fraction
X_{H_2O}	=	water vapor mole fraction
x	=	height above the burning surface, cm

I. Introduction

OBTAINING the structure of solid rocket propellant plumes is important for designing and validating new compositions and for establishing safety protocols in the event of accidents. In particular, an accurate estimate of the temperature and composition during combustion at atmospheric conditions is required so that radiation heat fluxes to the surroundings can be calculated in the event of an accidental fire during production and transport or due to engine malfunction during launch operations. In many monopropellant fuels, a metal such as aluminum is added to the oxidant and fuel binder to achieve high impulse [1]. For a composite propellant with 71% ammonium perchlorate, 18% aluminum, and 11% hydrocarbon binder, the estimated adiabatic equilibrium thermodynamic temperature for rocket motor conditions (68 atm) is 3574 K and that for burning at 1 atm is 3100 K. The resulting intermediate combustion of the propellant ammonium perchlorate and hydrocarbon fuel binder produces a mixture of gases (primarily CO_2, CO, H_2O, H_2, HCl, and N_2) and molten aluminum agglomerated particulate [2]. An estimated gas temperature at the propellant burning surface is 2286 K. Subsequent delayed reaction of the molten aluminum agglomerate in the gas plume produces a very luminous diffusion flame surrounding the aluminum particles [2]. The temperatures achieved within these diffusion flames [1] can be higher than 3000 K, severely limiting the opportunity for intrusive measurement techniques. Therefore, most experimental studies have focused on using nonintrusive optical methods to determine the structure of these flames [3]. One of the challenges associated with determining the interior structure of these flames is the very high radiation intensities from aluminum oxide (Al_2O_3) particles [4] causing the flame to be nearly opaque at far infrared wavelengths. There have been numerous studies that have documented the optical properties of Al_2O_3 within rocket plumes [3,4]. Laredo and Netzer [4] stated that most of the particles (greater than 95%) within the plume are less than 1 μm, and radiation intensity is dominant at the 3–5-μm band. In addition, they determined that the overall emissivity of the particles range from 0.19 to 0.35. Gryvnak and Burch [5] measured the emission from a small rocket plume at temperatures above and below the melting point and concluded that there is a large increase in the emissivity of the Al_2O_3 when melting. In addition, impurities play a significant role in determining the emissivity of the particulate [6]. Konopka et al. [7] provided experimental data on the refractive indices of particles. All of these studies pointed out that there is a wide variation in the optical properties of Al_2O_3 particulate within a solid rocket plume. Therefore, it is important that further characterization of optical properties of particulates are undertaken for accurate modeling of radiation from plumes and for estimating the flame's structure from radiation signatures [7,8].

Despite the lack of consensus on the optical properties of Al_2O_3, it is important to use existing values to obtain structure information, albeit with a higher degree of uncertainty, so that limits on the radiation loading caused by solid rocket propellant fires are understood. One method of determining the local structure information in particulate laden combustion flow is optical tomography. Absorption [9], emission [10], and combined absorption/emission [11] tomography have been used to obtain

Received 7 November 2006; revision received 16 April 2007; accepted for publication 3 May 2007.

*Technical Director, 1291-A Cumberland Avenue.
†Vice President, Applications, 1291-A Cumberland Avenue.
‡Senior Member, Technical Staff, 4800 Oak Grove Drive, Mail Stop T1702, Member AIAA.
§Principal Member, Technical Staff, 4800 Oak Grove Drive, Mail Stop 79-24.

structure information in hydrocarbon flames. Deconvolution algorithms based on the maximum likelihood estimation (MLE) method [12] have shown that converged local properties can be obtained as long as the equations are linear and have a positivity constraint. A linearized equation of radiative transfer [13] has been used with fan beam emission tomography (FBET) [14] to obtain local properties in hydrocarbon flames.

Based on the preceding studies, the objective of this study was to determine if fan beam emission tomography can be used to estimate the interior structure of ambient atmosphere solid rocket propellant plumes using existing optical properties of Al_2O_3.

II. Experimental Methods

FBET [14] is used to obtain the local properties within a flame based on measurements of path-integrated spectral radiation intensities at multiple view angles or projections. The present experiments were done using a generic 18% aluminized, 71% ammonium perchlorate, 11% hydroxyl terminated polybutadiene binder propellant.

For the burning of nominal 2.54-cm-diam, 1.27-cm-long strands of the composite solid rocket propellant, two spectrometers placed orthogonal to each other were used to obtain the measurements. A schematic diagram of the experimental arrangement is shown in Fig. 1.

Each spectrometer (Spectraline, Inc., model ES100) had a 1-D scanner (Spectraline, Inc., model SS100) in front of it. The ES100 spectrometer measures the spectral radiation intensities at 160 wavelengths ranging from 1.3 to 4.8 μm, with a spectral resolution of approximately 22 nm. Each spectra is obtained at 1320 Hz. The SS100 scanner is used to change the view angle of the spectrometer through a fan angle of approximately 20 deg in 128 discrete steps. The total time to collect one complete data set (full planar measurement) is therefore approximately 97 ms. A photograph of the ES100 with scanner is shown in Fig. 2.

The two spectrometers were placed in the same horizontal plane and perpendicular to each other. The spectrometers were approximately 20 cm from the center of the burner. The 2.54-cm-diam by 1.27-cm-long propellant strands were placed in the center of the burner. The burn time for the strands was approximately 16 s. Data were collected during the entire burn time. The spectral radiation intensities at any axial location first increase with time and then reach a relatively steady-state value during the last 6.4 s of the burn. Therefore, the last 6.4 s of the data were averaged to provide the mean spectral radiation intensities.

A photograph of the experimental arrangement is shown in Fig. 3, in which the data acquisition system is labeled as DAQ. The composite propellant was placed in a cup burner and ignited at the top using an electrically heated ignitor wire. The data collection was triggered by the ignition event. The composite propellant was inhibited on the side so that the plume was almost vertical in orientation. Measurements of spectral radiation intensities were obtained at four axial height locations (6.35, 12.7, 19.1, and 25.4 cm) above the initial top surface of the propellant. The burn rate of the propellant was about 0.8 mm/s at ambient pressure at an elevation of approximately 430 m. The measurements were obtained at one location per strand burn. Therefore, a total of four strands were burned to obtain the data set. A close-up photograph of the cup burner is shown in Fig. 4.

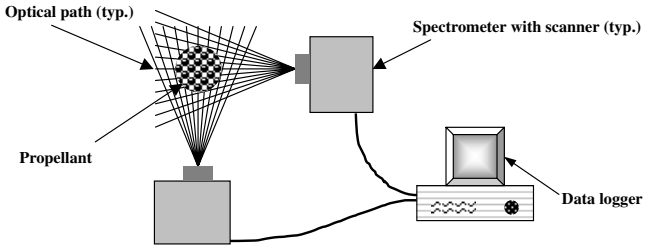

Fig. 1 Schematic diagram of the fan beam emission tomography experiment.

Fig. 2 Photograph of the ES100 spectrometer with the SS100 scanner.

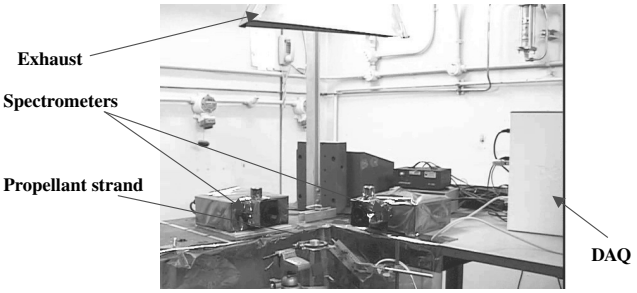

Fig. 3 Photograph of the experimental arrangement.

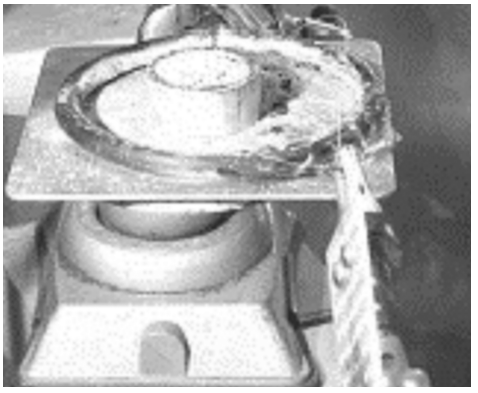

Fig. 4 Photograph of the cup burner.

III. Theoretical Methods

Tomographic reconstruction of local scalar properties is based on the deconvolution of a finite number of path-integrated measurements. The first task in developing the algorithm is to define the domain and the grids within the domain. The deconvolution method is explained using an axisymmetric system for clarity. For the axisymmetric system, the domain of deconvolution is illustrated in Fig. 5.

Each of the grids in the domain is a concentric ring. For ease of explanation, only two homogeneous rings are shown in Fig. 5. For each ring, unique scalars (temperature and the mole fractions of CO_2 and H_2O) are defined. In the FBET system, 128 rings are used for the

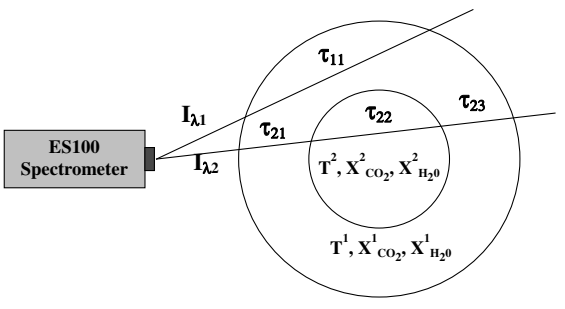

Fig. 5 Domain of deconvolution for an axisymmetric system.

deconvolution. In Fig. 5, the temperature and the mole fractions of CO_2 and H_2O are denoted as T^i, $X^i_{CO_2}$, and $X^i_{H_2O}$ respectively, where i denotes the ring number.

The spectral radiation intensity I_λ emitted from a homogeneous path at a specific wavelength l is given by the radiative transfer equation (RTE) as follows:

$$I_\lambda = I_{\lambda b}(1 - \tau_\lambda) \tag{1}$$

where $I_{\lambda,b}$ is the Planck function (dependent on the gas temperature), and τ_λ is the spectral transmittance of the homogeneous path. For a given temperature and mole fractions of CO_2 and H_2O, the spectral transmittance τ_λ along the optical path can be calculated using the narrow band radiation model RADCAL [15]. The two measured path-integrated intensities are obtained from the following equations:

$$I_{1,\lambda b}\left(1 - \tau_{11}^{R/\Delta_{11}}\right)\left[\frac{(1 - \tau_{11})}{(1 - \tau_{11}^{R/\Delta_{11}})}\right] = I_{1,\lambda} \tag{2}$$

$$I_{1,\lambda b}\left(1 - \tau_{23}^{R/\Delta_{23}}\right)\left[\frac{(1 - \tau_{23})\tau_{22}.\tau_{21} + (1 - \tau_{21})}{(1 - \tau_{23}^{R/\Delta_{23}})}\right] + I_{2,\lambda b}\left(1 - \tau_{22}^{R/\Delta_{22}}\right)\left[\frac{(1 - \tau_{22})\tau_{21} + (1 - \tau_{21})}{(1 - \tau_{22}^{R/\Delta_{22}})}\right] = I_{2,\lambda} \tag{3}$$

where R is radius of the domain, Δ_{ij} are the path lengths at each segment, subscript i refers to the measurement at view angle i, and subscript j refers to the segment number along the radiation path at view angle i.

The transmittances for two different path lengths with the same absorption coefficient can be obtained from Beer's law, as follows:

$$\tau_{11} = \exp\left(-k^1 \Delta_{11}\right) \tag{4}$$

$$\tau_{23} = \exp\left(-k^2 \Delta_{23}\right) \tag{5}$$

where k^1 is an absorption coefficient within ring 1. Using Eqs. (4) and (5), the relationship between the transmittances for the two segments can be obtained as follows:

$$\tau_{11}^{R/\Delta_{11}} = \tau_{23}^{R/\Delta 23}$$

The path-integrated intensities [right-hand side of Eqs. (2) and (3)] are available from the measurements at several wavelengths. In addition, the transmittances of all of the individual segments are available (known from the previous iterations or from the initial guess). Therefore, the two unknown quantities in Eqs. (2) and (3) are $I_{1,\lambda b}(1 - \tau_{11}^{R/\Delta_{11}})$ and $I_{2,\lambda b}(1 - \tau_{22}^{R/\Delta_{22}})$, the local spectral intensities. This is a linear system of equations with two unknowns. The maximum likelihood estimation [12] method is best suited for this problem because of its guaranteed convergence and ease of implementation. In Eqs. (2) and (3), the transmittances for all segments are obtained from the previous iteration.

Once the local intensities are known, the second step in the process is to use a linearized radiative transfer equation [13] (LRTE) in conjunction with the MLE method to obtain the local temperatures, gas concentrations, and particulate volume fraction of each individual segment. The second step assumes that the local intensities arise from a homogeneous gas layer. Obtaining the temperatures, gas concentrations, and particulate volume fractions from the local intensities has been published before [13] and the details are not provided here. The estimated local temperatures, gas mole fractions, and particulate volume fractions are used to calculate the transmittances for all segments in the domain. These transmittances are used then reused in step 1. The two-step process is continued until convergence is achieved. At the first iteration, local intensities are found only considering emission and neglecting self-absorption by intervening gaseous components.

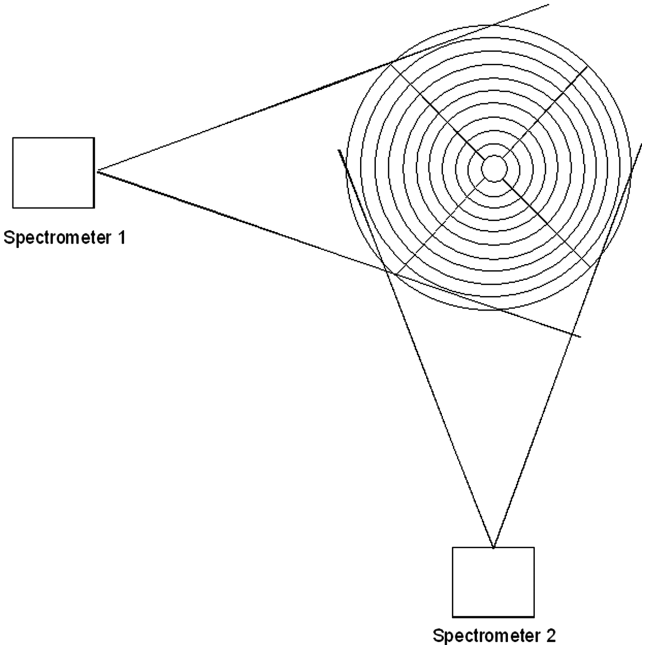

Fig. 6 Domain of deconvolution used with the FBET system.

To summarize, obtaining the solution to the deconvolution process consists of two steps:

1) Calculate the local spectral radiation intensities for all homogeneous rings, given the value of the transmittances for all segments in the optical path, using the MLE method [12].

2) Estimate the temperature, mole fractions of CO_2 and H_2O, and the particulate volume fraction from the local spectral intensities within each homogeneous ring using LRTE [14]. The local properties are used to recalculate the transmittances of each path in the deconvolution domain and reused in step 1.

The measurements at the Jet Propulsion Laboratory (JPL) were taken at two view angles using two spectrometers. Each spectrometer measures 128 points over a single span and 160 wavelengths for each point; therefore, the angular resolution of the measurements is 90 deg. The domain of deconvolution and the grids used are shown in Fig. 6.

The additional piece of information required to complete the deconvolution is the absorption coefficients of the gases and the Al_2O_3 particulate. The absorption coefficients of the gases are obtained from the RADCAL [15] database. The absorption coefficient of the particulate was obtained from a representative set of published values [7,16]. For obtaining aluminum oxide temperatures and particulate volume fractions, the spectral radiation intensities at three narrow regions (1.6 to 1.75, 2.1 to 2.35, and 3.45 to 3.9 μm) were used. To obtain gas temperatures and concentrations, the spectral radiation intensities from 4.35 to 4.8 μm were used.

IV. Results and Discussion

The spectral radiation intensity profiles obtained from one of the tests (6.35 cm above the initial top surface of the propellant) are shown in Fig. 7. The water vapor band at 2.7 μm and the carbon dioxide band at 4.4 μm are identified in Fig. 7.

The spectral radiation intensities are zero at the edges of the flame and increase toward the center. It is clearly evident from the figure that the plume is not axisymmetric. Radiation from molten aluminum is expected to be very low at these wavelengths due to the very low emissivity of molten aluminum.

These spectral radiation intensities were used in the deconvolution algorithm to obtain particulate concentrations, particulate temperatures, carbon dioxide concentrations, and gas temperatures. The gas temperatures obtained from the flame are shown in Fig. 8. All measurements were obtained using a 2.54-cm-diam, 1.27-cm-long

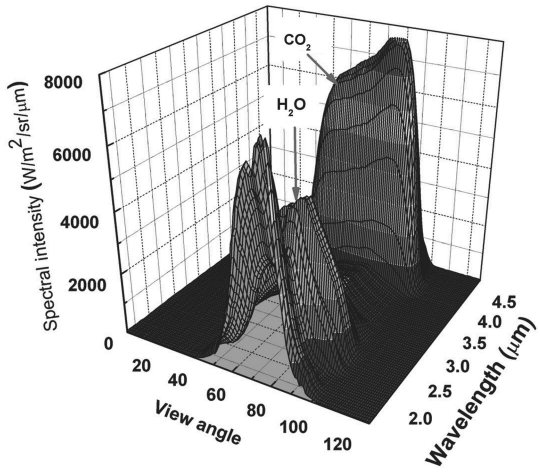

Fig. 7 Sample spectra obtained from the FBET system.

propellant strand. The extent of the propellant surface is marked in the subsequent figures with small vertical solid lines on the *x* axis.

Theoretically, close to the burn surface, the gas temperature should be similar to the adiabatic flame temperature with none of the aluminum being burned (∼2280 K). Far from the burn surface (on the order of 1 m), the gas temperature should be similar to the adiabatic flame temperature with all of the aluminum being burned (∼3100 K). The temperature at 6.3 cm is higher than what might be expected. Because the size distribution for the aluminum particles leaving the burn surface is bimodal, it is likely that the fine particles have all reacted to oxide within a distance of 6.3 cm, thereby raising the gas temperature (for ∼10% aluminum burned ∼2320 K). For an adiabatic process, the temperature at 25 cm should be greater than at 6.3 cm, because the energy from the oxidation of aluminum is transferred to the gas. Apparently, the radiation losses exceed the energy from the aluminum oxidation reaction.

Presumably, if the plume cross section were larger, it may become more opaque in the spectral band emitted by the aluminum suboxides or molten alumina, thereby reducing the radiation losses. The plume also flows into ambient air, which is displaced and also becomes entrained. The plume flow can be expected to be turbulent, and the entrained air at ambient temperature will significantly cool the plume. However, the oxygen in the air can also react rapidly with the aluminum agglomerate to produce a very luminous surrounding diffusion flame (adiabatic temperature ∼3500 K at oxygen stoichiometry) when the agglomerate passes into air.

The tomography data show that the gas temperatures have a roughly parabolic profile and get flatter with distance from the top of the propellant burning surface, as expected from the preceding discussion. The peak gas temperature at an axial distance of 6.3 cm from the initial propellant burn surface is approximately 2900 K. At an axial distance of 25 cm, the peak gas temperature has dropped by 100 to about 2800 K, and at the center of the plume, the temperature is about 2600 K. The peak temperature of 2900 K is lower than previous calculations of the adiabatic flame temperature of 3100 K for aluminized solid rocket propellants when all of the aluminum is burned [17]. However, this is to be expected because not all of the aluminum has burned, and a significant amount of the formulated aluminum fuel is contained in the largest agglomerates, which burn for a long time or distance. At an axial distance of 12.7 cm, the

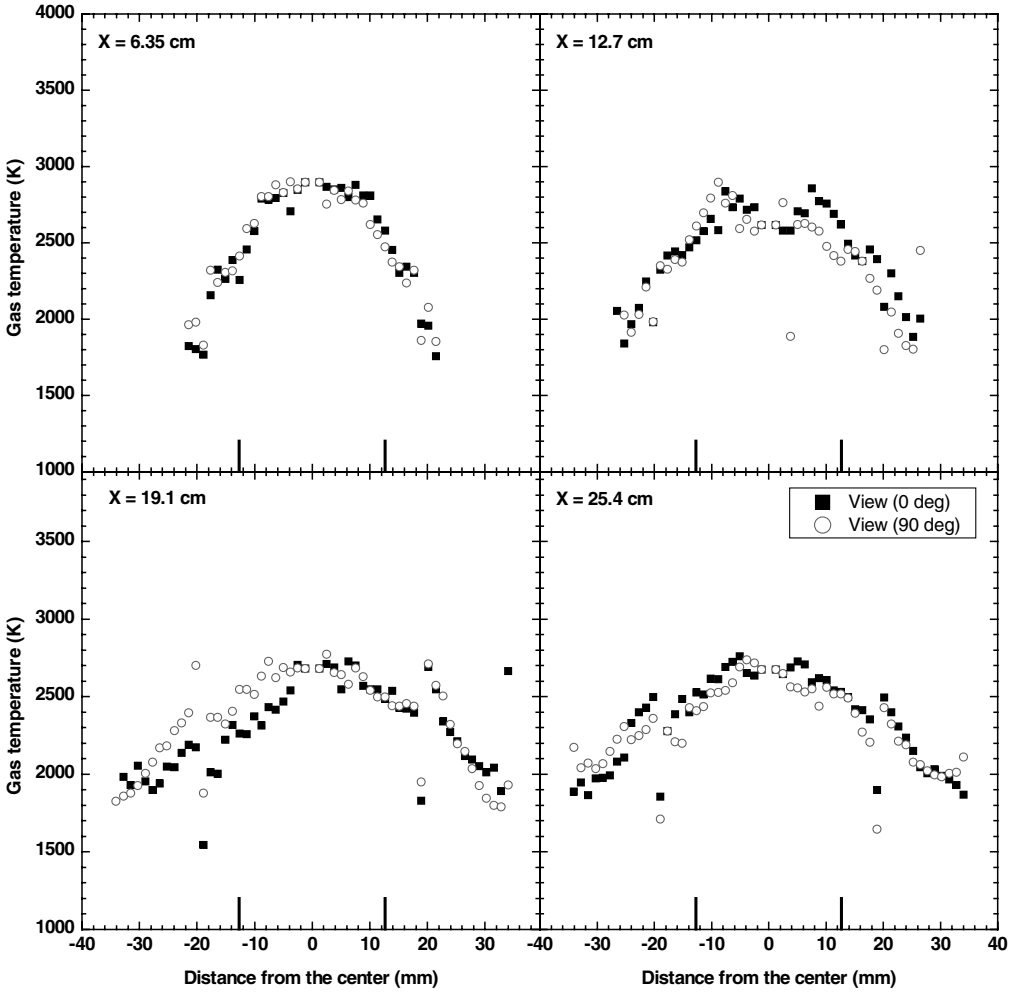

Fig. 8 Gas temperatures at four axial height locations within the plume.

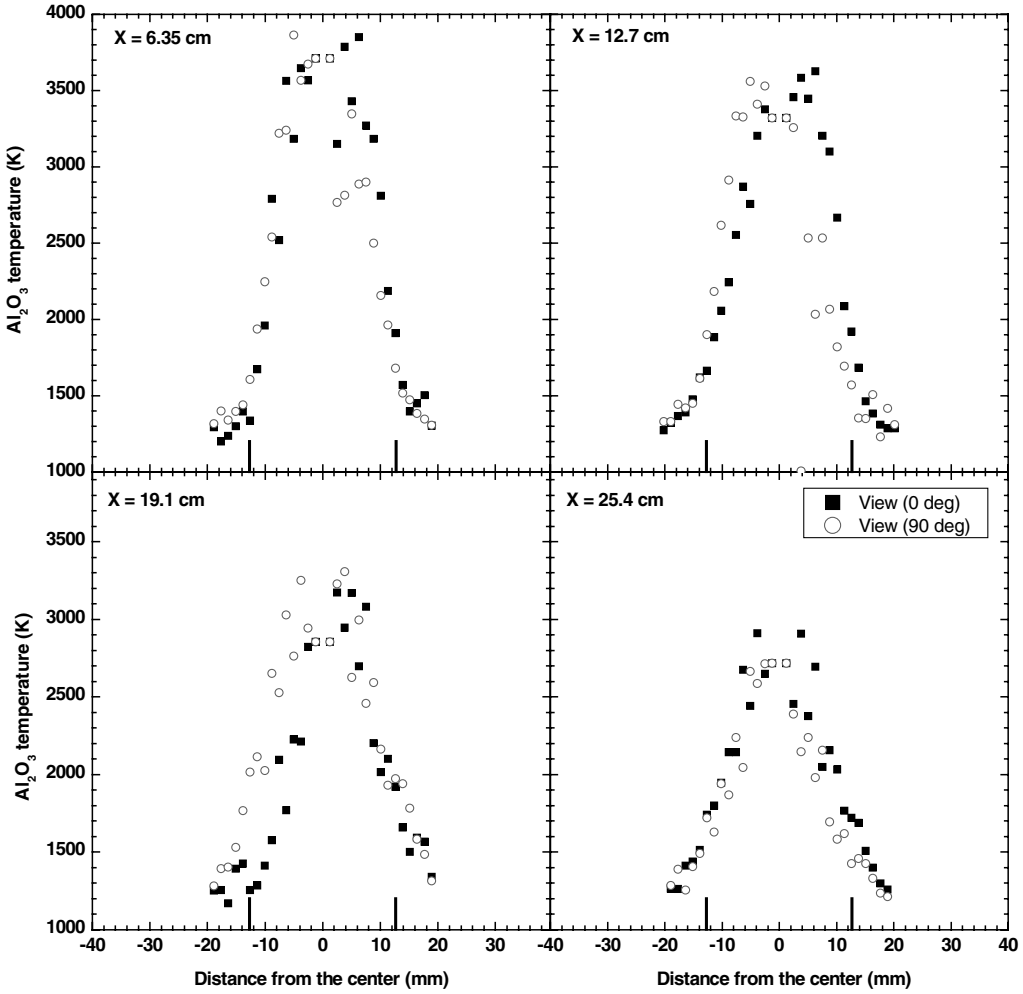

Fig. 9 Aluminum oxide particulate temperatures at four axial height locations within the plume.

decrease in the center temperature is believed to be significant and it is closer to the expected 2600 K. Similar decreases in temperature also occur at axial distances of 19 and 25 cm.

The location of the peak temperature (2900 K at an axial distance of 6.3 cm from the initial propellant surface) is inconsistent with the fact that the oxidation of aluminum (the reaction that raises the adiabatic flame temperature from about 2300 K at the burning surface to 3100 K, when the aluminum is completely oxidized) occurs over distances of approximately a meter from the initial propellant surface. The gas temperatures are not axisymmetric, with significant differences seen in the four quadrants of the plume. The spread in temperatures and flattening of the plot with lower values from ~2800 K at the edge of the propellant plume to ~2000 K at the center can be attributed to mixing with air and cooling of the plume by radiation to the surroundings. There is a little bit of scatter in the data, which is probably due to the inherent unsteadiness of the flame. A longer period of sampling may reduce the scatter in the data. Despite these drawbacks, this is the first time that radial profiles of gas temperatures have been obtained in solid rocket propellant fires at ambient pressure.

The corresponding aluminum oxide particulate temperatures for the same locations are shown in Fig. 9. The aluminum oxide particulate temperatures are significantly higher than the gas temperatures and are consistent with adiabatic calculations of aluminum combustion in air [17] or in oxygen. Close to the burning propellant surface, temperatures are higher than 3500 K. However, there is little reason to believe that a significant amount of air is entrained at the 6.3-cm height at the center of the plume. The high temperatures measured are more consistent with the 3800 K discussed by Price et al. [18] in the high-temperature zone of the detached flame envelope around each of the aluminum droplets, referred to as the diffusion flame, as follows:

> In this flame envelope, the most energetic step is the formation of Al_2O_3 in liquid form, primarily on the surface of the existing smoke droplets in that envelope. It is the resulting energy of that reaction, and the corresponding high temperature of these smoke droplets, that makes the combustion so luminous.
>
> Indeed, these droplets are near their boiling temperature, and it is partly because of the radiative disposal of energy that the rate of formation of liquid Al_2O_3 can exceed the rate of its vaporization.[¶] At 1 atm this process maintains the Al_2O_3 temperature at about 3800 K.

In addition, the temperatures drop very rapidly at the plume center with downstream plume distance: 3850, 3700, 3200, and 2900 K. This is believed to be primarily due to the strong radiative cooling of the aluminum oxide particles. The aluminum oxide particulate temperatures also decrease significantly to the range of 1200 to 1750 K after apparently mixing with surrounding ambient air at the perimeter of the plume.

The CO_2 mole fractions at the four axial height locations are shown in Fig. 10.

The CO_2 concentrations from adiabatic equilibrium thermodynamic calculations are as follows: At the propellant burning surface, the CO_2 mole fraction is 0.106 when there is no aluminum burned. When 50% of the aluminum is burned, the CO_2 is predicted to be 0.044. When 100% of the aluminum is burned, the CO_2 mole fraction is predicted to be 0.016. These estimates are for chemical equilibrium, which may not occur locally in the plume. The gas concentration profiles are also not axisymmetric. In fact, the asymmetry in the gas concentration profiles is greater than that in the temperature profiles. The cause for the greater degree of asymmetry

[¶]Al_2O_3 dissociates instead of boiling, and the high energy of formation can be realized only if the heat is being removed to keep the temperature down.

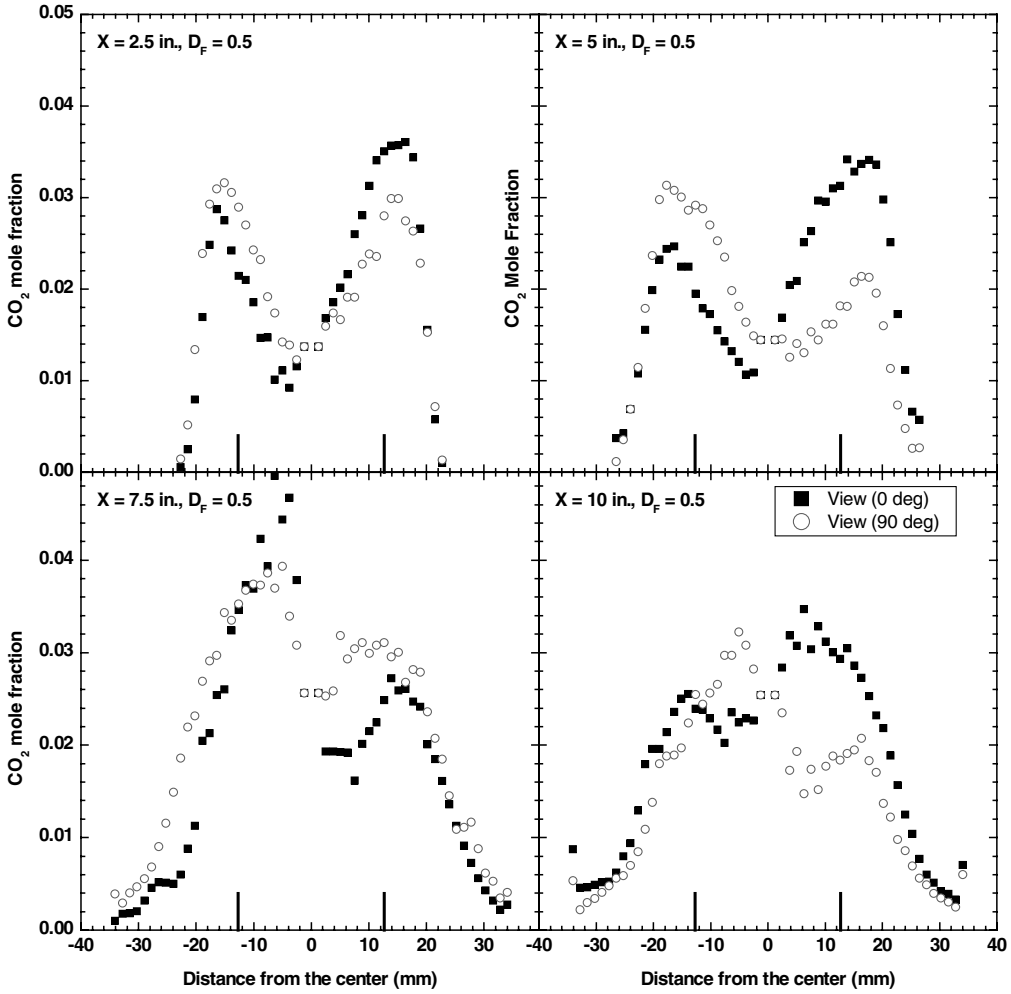

Fig. 10 CO_2 gas concentrations at four axial height locations within the plume.

in the gas concentrations is not readily apparent unless one conjectures that the ammonium perchlorate and binder reaction gas products are not well-mixed and that there is significant entrained air due to plume turbulence.

The significant decrease in the mole fraction at the center of the plume is to be expected. The CO_2, and H_2O in the plume react with the aluminum particulate in a diffusion flame and at the aluminum agglomerate surface to form CO and H_2. Thus, the CO_2 concentration should decrease. The CO_2 concentration should increase when the plume mixes with ambient air ($CO + \text{air}\, O_2 \Rightarrow CO_2$) as the plume rises upward along with entrained air.

However, the CO_2 mole fraction numerical values do not correlate with the theoretical chemical equilibrium calculations. In all four burns, the large-diameter agglomerate aluminum fraction, which contains most of the aluminum, is ignited and burning with a diffusion flame, but has not completely burned at 25 cm above the burning propellant surface. Thus, the CO_2 reduction to CO is significantly less than could have occurred (from the expected value of $\sim$0.106 to $\sim$0.016 mole fraction, as actually measured). In conclusion, the CO_2 mole fraction data agree with some expected results, but additional data will be needed to resolve the difference between the experimental CO_2 low mole fraction values and the theoretical values. It is conjectured that the CO_2 mole fraction may be biased by local conditions at the aluminum agglomerate diffusion flame, in which equilibrium concentrations may not occur.

The aluminum oxide particulate concentrations at the four axial locations are shown in Fig. 11. The expected volume fraction of alumina particulate in the plume is 5.4 ppmv at 2900 K and 15.5 ppmv cooled to 1000 K. This is within the range of the data in Fig. 11. The data at the 6.3-cm axial height appear to dip in the center, where the gas temperature is highest and air mixing is minimal, with the 3–7-ppmv range being correlated and reasonable. The data at the 12.7-cm height from a different burn show the same characteristic values. For the data at a height of 19 cm, it is conjectured that the high of 14 to 18 ppmv at -10-mm distance from the center is due to quasi-steady-state mixing with air. In the turbulent mixing with cool air, the gas temperature decreases and the molar volume is also decreased. At a 25-cm height, the data show the dip with high temperature and the increase in concentration with entrained air that cools the plume at the perimeter.

The radial profiles of the particulate concentrations have a much higher degree of scatter than either the gas concentrations or the temperature measurements. This higher degree of scatter is primarily caused by the high uncertainty in the absolute values of the refractive indices.

It should be noted that only the absolute values of refractive indices play a role in the alumina particulate concentration estimation. For alumina particulate temperatures, it is the variation of refractive indices that play a more significant role. The sensitivity of the estimated temperatures and particulate concentrations to variation in both the absolute values of refractive indices and the slopes of the refractive indices were calculated.

In general, a 20% increase in the particulate absorption coefficient increases the estimated temperatures by a few degrees and the estimated particulate volume fraction by approximately 20%. This is not surprising because temperature is estimated using multi-wavelength matching of the spectra, and changes in absolute values of the absorption coefficient, although retaining the spectral characteristics, do not change the estimated temperatures significantly.

A 20% variation in the slope of the absorption coefficient can change the estimated temperatures by approximately 50 deg and the

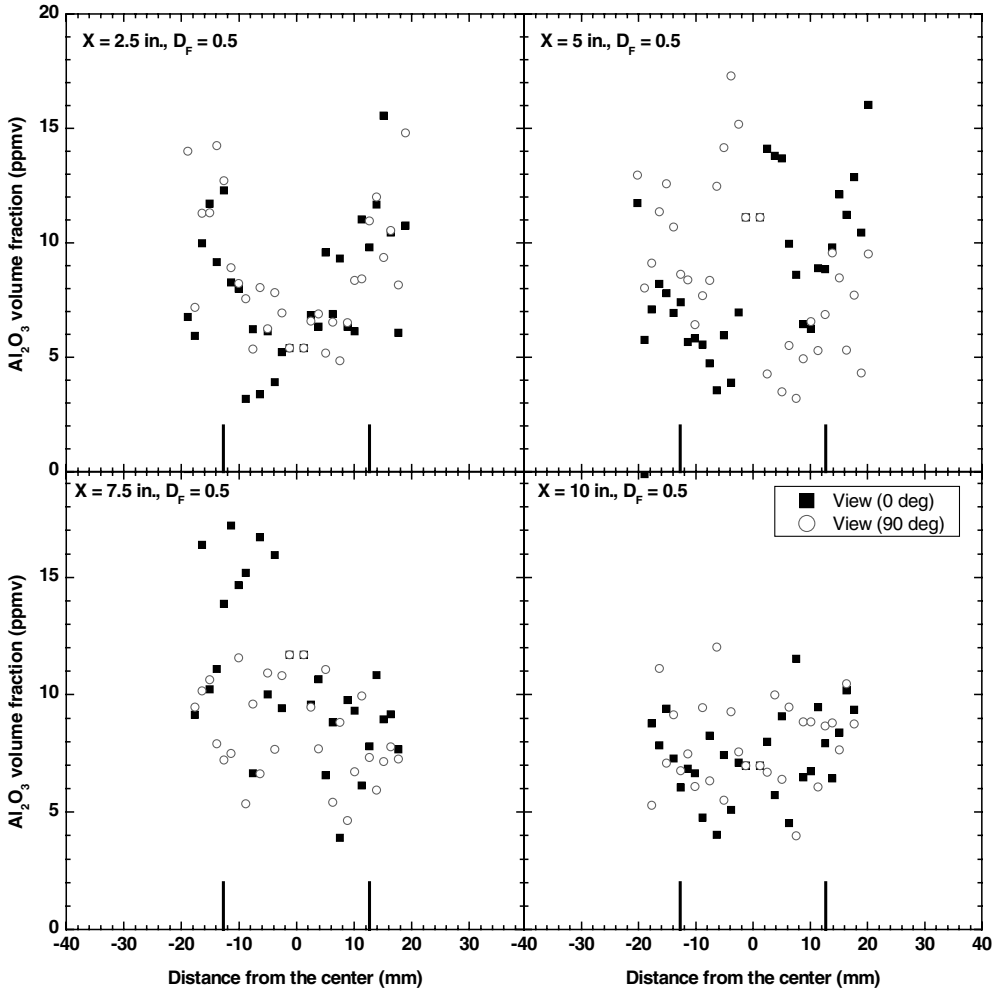

Fig. 11 Aluminum oxide particulate concentrations at four axial height locations within the plume.

estimated volume fractions by as much as 30%. Therefore, it is crucial to use the correct slopes for the spectral absorption coefficients of particulate when estimating temperatures and volume fractions using emission spectroscopy.

V. Conclusions

The following conclusions can be drawn from the present study:

1) The feasibility of the FBET system in estimating radial profiles of particulate and gas temperatures and their concentrations in solid rocket propellant plumes was conclusively demonstrated.

2) The aluminum oxide particulate temperatures, consistent with those previously reported in the literature, are significantly higher than the gas temperatures and showed higher effects of radiative cooling.

3) The gas concentrations and temperatures obtained in the present study are consistent with values that have been reported previously in the literature and with adiabatic chemical equilibrium thermodynamic calculations, except for the CO_2 mole fraction.

4) The particulate temperature and volume fraction estimates are sensitive to the slope of the absorption coefficient in the infrared regions of the spectra. The temperature is insensitive to absolute changes in the value of the absorption coefficient, as long as the variation of the absorption coefficient with wavelength is maintained at a constant value.

5) The local structure within solid rocket propellant fires was estimated for the first time using an optical diagnostic method.

Acknowledgments

This research was partially performed at the Jet Propulsion Laboratory (JPL), California Institute of Technology, under a contract with NASA. The work at En'Urga, Inc. was conducted under contract no. 1274328 from the JPL. Y. Sivathanu and. J. Lim would like to thank JPL for the support provided for their work. The authors thank R. G. Webster, W. Gavid, and T. A. Slager for their assistance during the experiments and H. Li and W. L. Dowler for supporting analysis and discussions.

References

[1] Duval, R., Soufiani, A., and Taine, J., "Coupled Radiation and Turbulent Multiphase Flow in an Aluminised Solid Propellant Rocket Engine," *Journal of Quantitative Spectroscopy & Radiative Transfer*, Vol. 84, No. 4, 2004, pp. 513–526.

[2] Sabnis, J. S., "Numerical Simulation of Distributed Combustion in Solid Rocket Motors with Metalized Propellant," *Journal of Propulsion and Power*, Vol. 19, No. 1, 2003, pp. 48–55.

[3] Reed R. A., and Calia, V. S., "Review of Aluminum Oxide Rocket Exhaust Particles," 31st AIAA Aerospace Sciences Meeting, AIAA Paper No. 93-2819, 1993.

[4] Laredo, D., and Netzer, D. W., "The Dominant Effect of Alumina on Nearfield Plume Radiation," *Journal of Quantitative Spectroscopy & Radiative Transfer*, Vol. 50, No. 5, 1993, pp. 511–530.

[5] Gryvnak, D. A., and Burch, D. E., "Optical and Infrared Properties of Al_2O_3 at Elevated Temperatures," *Journal of the Optical Society of America*, Vol. 55, No. 6, 1965, pp. 625–631.

[6] Pluchino, A. B., and Masturso, D. E., "Emissivity of Al_2O_3 Particles in a Rocket Plume," *AIAA Journal*, Vol. 19, No. 9, 1981, pp. 1234–1237.

[7] Konopka, W. L., Reed, R. A., and Calia, V. S., "Measurements of Infrared Optical Properties of Al_2O_3 Rocket Particles," *Spacecraft Contamination: Sources and Prevention*," Progress in Astronautics and Aeronautics, Vol. 91, AIAA, New York, 1984, pp. 180–196.

[8] Nelson, H. F., "Evaluation of Rocket Plume Signature Uncertainties," *Journal of Spacecraft and Rockets*, Vol. 24, No. 6, 1987, pp. 546–551.

[9] Santaro, R. J., Semerjian, H. G., Emmerman, P. J., and Goulard, R.,

"Optical Tomography for Flow Field Diagnostics," *International Journal of Heat and Mass Transfer*, Vol. 24, No. 7, 1981, pp. 1139–1150.

[10] Uchimaya, H., Nakajima, M., and Yuta, S., "Measurement of Flame Temperature Distribution by IR Emission Computed Tomography," *Applied Optics*, Vol. 24, No. 23, Dec. 1985, pp. 4111–4115.

[11] Best, P. E., Chien, P. L., Carangelo, R. M., Solomon, P. R., Danchak, M., and Ilovici, I., "Tomographic Reconstruction of FT-IR Emission and Transmission Spectra in a Sooting Laminar Diffusion Flame: Species Concentrations and Temperatures," *Combustion and Flame*, Vol. 85, No. 3, 1991, pp. 309–318.

[12] Vardi, Y., and Lee, D., "From Image Deblurring to Optimal Investments: Maximum Likelihood Solutions for Positive Linear Inverse Problems," *Journal of the Royal Statistical Society, Series B (Methodological)*, Vol. 55, No. 3, 1993, pp. 569–612.

[13] Lim, J., Sivathanu, Y., Ji, J., and Gore, J., "Estimating Scalars from Spectral Radiation Measurements in a Homogeneous Hot Gas Layer," *Combustion and Flame*, Vol. 137, 2004, Nos. 1–2, pp. 222–229.

[14] Sivathanu, Y., Lim, J., and Feikema, D., "Fan Beam Emission Tomography for Laminar Fires," *Seventh International Workshop on Microgravity Combustion and Chemically Reacting Systems*, CP-2003-212376, NASA, Washington, D.C., 2003, pp. 237–240.

[15] Grosshandler, W. L., "Radiative Heat Transfer in Nonhomogeneous Gases: A Simple Approach," *International Journal of Heat and Mass Transfer*, Vol. 23, No. 11, 1980, pp. 1447–1459.

[16] Duval, R., Soufiani, A., and Taine, J., "Coupled Radiation and Turbulent Multiphase Flow in an Aluminised Solid Propellant Rocket Engine," *Journal of Quantitative Spectroscopy & Radiative Transfer*, Vol. 8, No. 4, 2004, pp. 513–526.

[17] Reinhart, L. E., Bowman, R. C., Jr., Li, H., Webster, R. G., Kulleck, J. G., Dowler, W. L., Eubank, C. A., and Fry, R. S., "Initial Characterization of Burning the Solid Rocket Propellant TP-H-3340 in Ambient Air," *Proceedings of JANNAF* [CD-ROM], 2005, Paper CS-4B-9.

[18] Price, E. W., Mayer, W. L., Strahle, W. C., Samant, S. S., Powell, E. A., Sigman, R. K., and Handley, J. C., "The Fire Environment of a Solid Rocket Propellant Burning in Air," U.S. Air Force Weapons Lab. Rept. TR-78-34, Kirtland AFB, NM, Mar. 1979, pp. 51–52.

R. Lucht
Associate Editor